Functional Topography of Rod and Cone Photoreceptors in Macaque Retina Determined by Retinal Densitometry

Gen Hanazono,[1,2] *Kazushige Tsunoda,*[1,2] *Yoko Kazato,*[1,2] *Wataru Suzuki,*[1,2,3] *and Manabu Tanifuji*[2]

PURPOSE. The purpose of this study is to determine the topography of bleaching in rods, middle/long-wavelength (M/L) and short-wavelength (S) cones in the macaque retina by using a modified retinal densitometry technique.

METHODS. A modified commercial digital fundus camera system was used to measure continuously the intensity of the light reflectance during bleaching with band pass lights in the ocular fundus of three adult Rhesus monkeys (Macaca mulatta) under general anesthesia. The topography of bleaching in rods, M/L-, and S-cones was obtained separately by considering the characteristic time course of the reflectance changes, depending on the wavelengths of light and retinal locations.

RESULTS. The distribution of M/L-cones response had a steep peak at the foveal center and was elongated horizontally. The distribution of rod responses was minimum at the foveal center and maximum along a circular region at the eccentricity of the optic disc. The distribution of S-cone responses was highest at the fovea and was excavated centrally. There was a circular region with the maximal responses at 0.38 to 1.0 degrees from the foveal center.

CONCLUSIONS. With the current imaging technique, not only the steep peak of the M/L-cone responses at the fovea, but the ring-shaped distribution of rod responses in the periphery and the central reduction of S-cone response could be determined with good resolution. (*Invest Ophthalmol Vis Sci.* 2012;53:2796–2803) DOI:10.1167/iovs.11-9252

The human visual system is a duplex system, consisting of a rod system for scotopic conditions and a cone system for photopic conditions. Three types of cones mediate color vision; long (L), middle (M), and short (S) wavelength-sensitive cones. The distribution of the photoreceptors has been well investigated on postmortem eyes of humans and macaques.[1–9] These studies reported the anatomical densities of the different types of photoreceptors, but the results did not necessarily reflect their functional properties. Psychophysical experiments also have been used to assess photoreceptor function.[10-15] However, the results reflect not only the retinal function, but the visual function from the photoreceptors to the visual cortex.

Approximately 50 years ago, the time course of the bleaching of photopigments was determined quantitatively by measuring the reflectance changes during bleaching and regeneration of the visual pigments in human retinas.[16-22] This method, retinal densitometry, was used to determine the in vivo kinetics of the photopigments of cones and rods quite accurately. The spatial distribution of the reflectance changes was determined later by examining images obtained by either a fundus camera or a scanning laser ophthalmoscope (SLO), that is, imaging fundus reflectometry.[23-33] With these techniques, the distribution of photoreceptors was mapped objectively and non-invasively as bleach-derived light reflectance changes in normal and diseased eyes. However, the responses of the different types of photoreceptors, especially rods and S-cones, could not be segregated accurately because the response time courses were not monitored accurately.

We developed a new retinal densitometry system that can measure the retinal reflectance changes continuously after bleaching with band pass lights in anesthetized rhesus monkeys. We found that the time course of the reflectance changes depended not only on the wavelength of light but on the retinal location. By using such characteristics, the topography of bleaching in rods, M/L-, and S-cones could be obtained separately. The circular region of the maximal rod responses and the reduction of S-cone responses in the center were determined functionally with good spatial resolution.

METHODS

The experiments were performed on three adult Rhesus monkeys (Macaca mulatta). Following an intramuscular injection of atropine sulfate (0.08 mg/kg), the monkeys were anesthetized with droperidol (0.25 mg/kg) and ketamine (5.0 mg/kg), and then paralyzed with vecuronium bromide (0.1 mg/ kg/ hour). To block pain, fentanyl citrate (0.83 μg/kg/h) was infused intravenously continuously throughout the experiments. The animals were ventilated artificially with a mixture of 70% N_2O, 30% O_2, and 1.0–1.5% of isoflurane. The electroencephalograms (EEGs), electrocardiograms (ECGs), expired CO_2, and rectal temperature were monitored continuously throughout the experiments. Before the recordings, the pupils were dilated fully with topical tropicamide (0.5%) and phenylephrine hydrochloride (0.5%). The experimental protocol was approved by the Experimental Animal Committee of the RIKEN Institute, and all experimental procedures were carried out in accordance with the guidelines of the RIKEN Institute and the ARVO Statement for the Use of Animals in Ophthalmic and Vision Research.
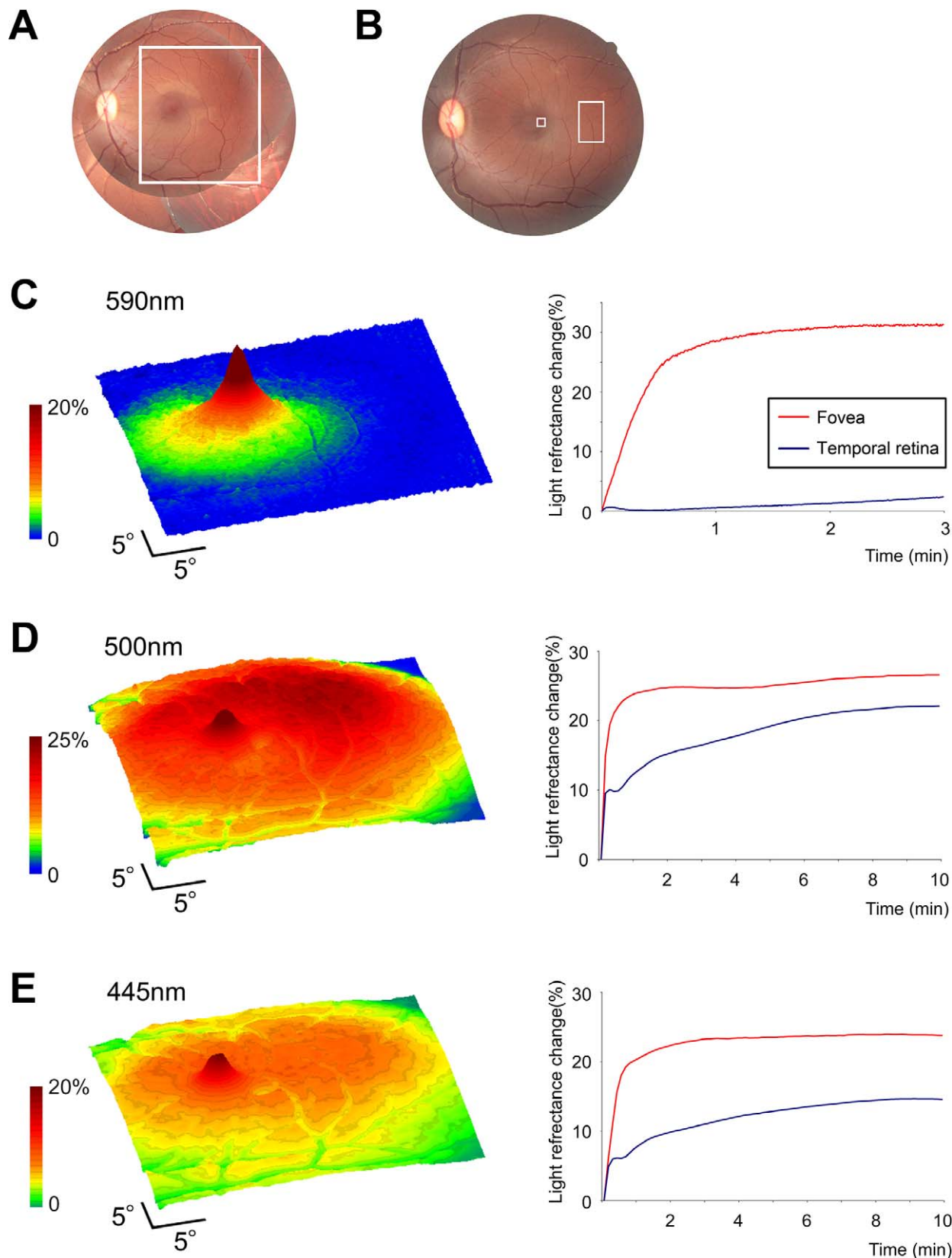
Figure 1. Bleach-induced light reflectance changes in retina by different wavelengths of light. (**A**, **B**) Regions in the macaque retina for the topographic (**A**) and time course analyses (**B**). A small square in **B** indicates the location of the fovea and a rectangle indicates the location of the temporal retina. (**C–E**) Pseudo-colored topographic map of the bleach-induced light reflectance changes (*left*), and time course in the fovea and temporal retina with high intensity light of 5.35 log phot. td for 590 nm (**C**), 6.54 log scot. tld for 500 nm (**D**), and 4.58 log phot. td for 445 nm (*right*) (**E**). Color scales indicate the reflectance changes (%) at the completion of each recording period relative to the reflectance at the beginning. Red lines indicate the time course at the fovea and blue lines for the temporal retina. Data from Monkey 1 are presented.

Rod response
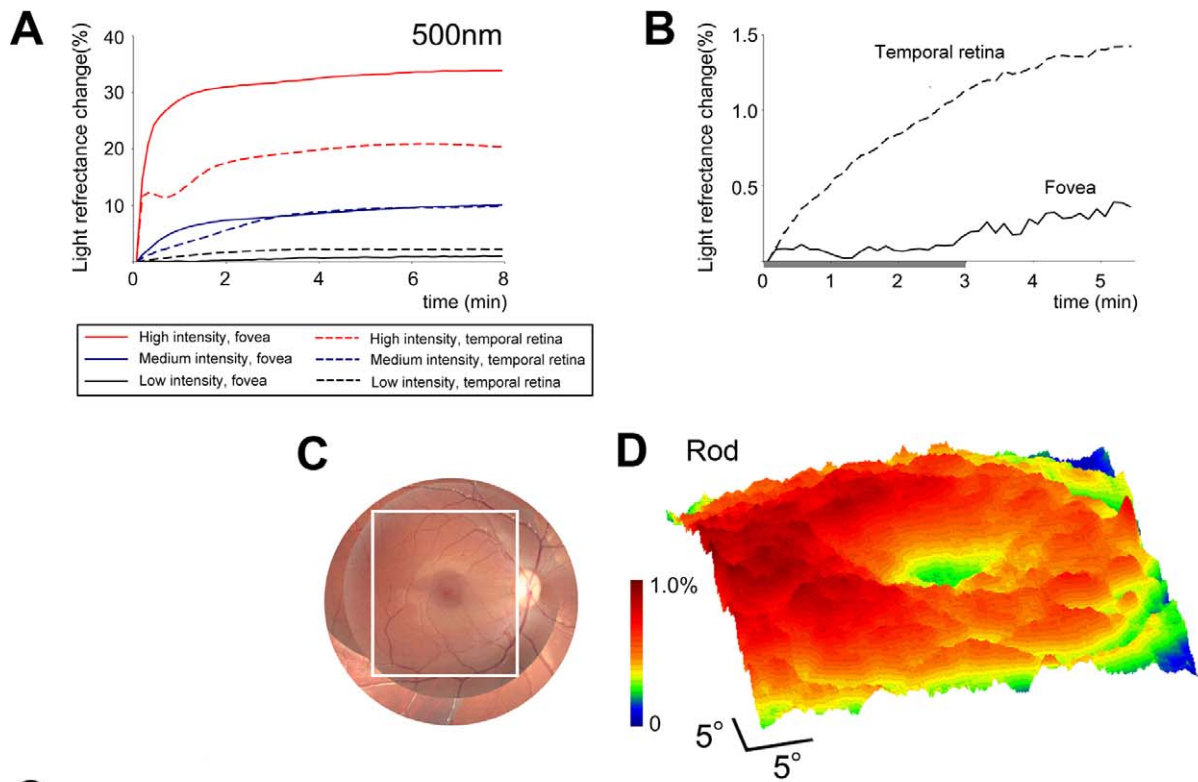
S-cone response
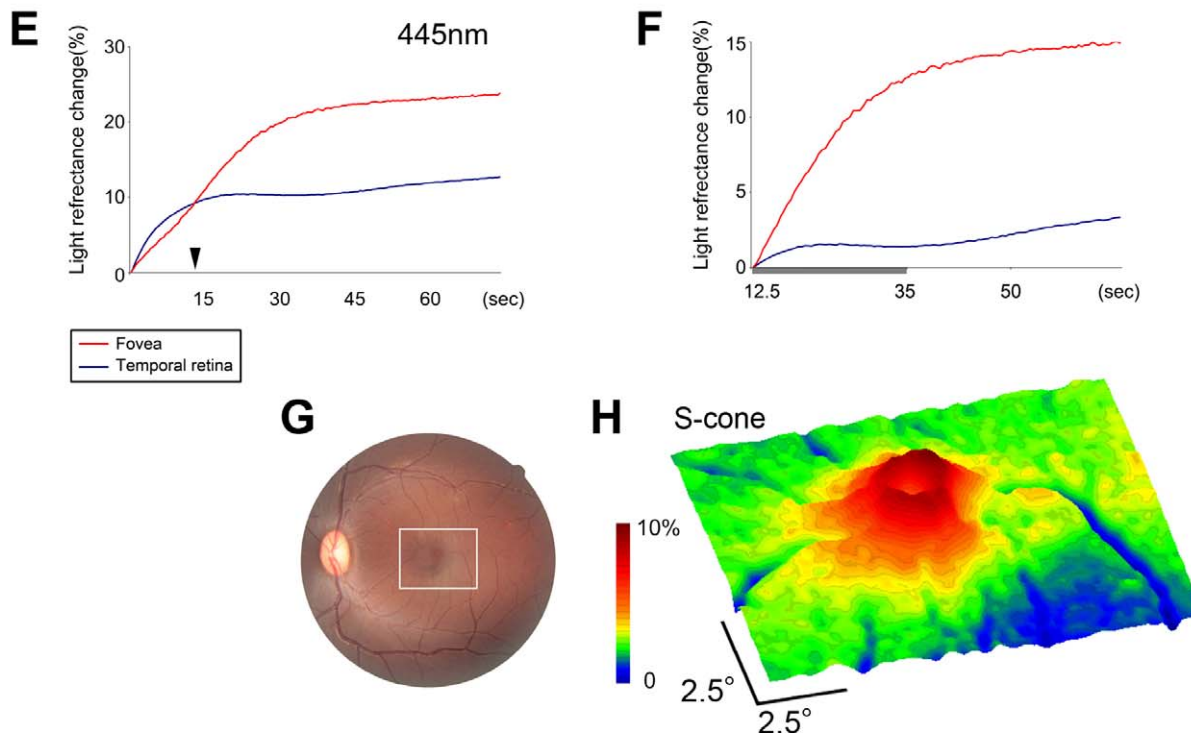
FIGURE 2.   Time-course analyses for the rod (**A–D**) and S-cone (**E–H**) responses. (**A**) Time courses for 500 nm at three different intensities; 6.54 log scot. tld for strong, 5.14 log scot. tld for medium, and 4.73 log scot. tld for weak intensity. Time course at the fovea is represented by solid lines and those at the temporal retina by dotted lines. (**B**) Expanded image of the time course for the weak 500 nm light (4.73 log scot. tld) for the initial five minutes. The response at the fovea remains flat during the initial three minutes. (**C, D**) Reflectance topographic map for weak 500 nm light (4.73 log scot. tld) during the initial three minutes (**D**) measured in the posterior-pole region in (**C**). The color scale indicates the reflectance changes (%) at 3 minutes. (**E, F**) Expanded time course for the 455 nm light for the initial 75 seconds (**E**), and re-plotted reflectance changes relative to the

Retinal Densitometry System and Data Analyses

A modified commercial digital fundus camera system (NM-1000, Nidek, Aichi, Japan) was used to observe and measure continuously the light reflectance changes from the ocular fundus. The fundus images were recorded with a CCD video camera (PX-30BC, Primetech Engineering, Tokyo, Japan), and the images were digitized with an IBM/PC-compatible computer equipped with a video frame grabber board (Corona II, Matrox, Quebec, Canada; gray-level resolution 10 bits, spatial resolution 640 × 480, temporal resolution 1/30 seconds). The optical pathway was modified to illuminate the entire posterior pole region homogeneously for 35 degrees in diameter by inserting a neutral density filter within the optical pathway that was conjugate to the retina. The density of the filter was the highest at the center and decreased gradually toward the periphery to compensate for the highest luminance along the optical axis, which is characteristic to commercial fundus cameras. With this filter, the differences of the estimated retinal luminances within the region of interest were within ± 10%.

Following dark adaptation for one hour, the fundus was illuminated continuously in the dark room with the light from a halogen lamp filtered through one of the three band pass interference filters: blue ($\lambda_{max} = 445 \pm 30$ nm) for S-cone, green ($\lambda_{max} = 500 \pm 15$ nm) for rods, and yellow ($\lambda_{max} = 590 \pm 15$ nm) for M/L-cones. Because the maximum absorption of the M and L cones was close, that is 535 nm for M-cones and 565 nm for L-cones, and differentiation between M- and L-cones in this method was technically difficult, we did not aim to segregate the response topography of these two types of cones. These cones thus were referred to as M/L-cones in this study.

The bleaching of the photopigments was measured as increases in light reflectance from the ocular fundus, that is a brightening. The time course of the reflectance changes was calculated as follows. The gray-scale values of the images obtained after the stimulus were divided, pixel by pixel, by those obtained during a 0.5-second period at the beginning of the trial. This ratio was rescaled to 256 levels of gray-scale resolution to show the stimulus-induced reflectance changes. In each trial, the reflectance was recorded for as long as 11 minutes, which is the maximum recording duration possible in our computer system. Spatial averaging (3 × 3 pixels, i.e. 0.15 × 0.15 degrees, for mapping M/L- and S-cones, or 5 × 5 pixels, i.e. 0.25 × 0.25 degrees, for rods) was performed to build up topographies of retinal responses.

For measuring the rod reflectance changes of the peaks not located in the macular region, six trials were performed consecutively to measure the light reflectance changes in different retinal locations (Fig. 3B). The topographies of these trials were merged to map the responses over 40 degrees in diameter.

We made measurements on three monkeys, and the results with unwanted physiological artifacts, such as the large decrease of reflectance along the vessels due to absorption by hemoglobin and pulsation-induced reflectance changes at the edge of the optic disk, were excluded from the response topographies.

RESULTS

Topography and Time Course of Maximum Bleaching for Each Band Pass Filter

We bleached the retina with different wavelengths of light, and the topographic distribution of the bleaching patterns with yellow (5.35 log phot. td), green (6.54 log scot. tld) and blue (4.58 log phot. td) are shown in Figure 2. The time course of

reflectance changes at the foveal area of 1.75 degrees in diameter and temporal retina 15.0 degrees from the center are shown. The light through the yellow (590 nm) filter bleached the M- and L- cones exclusively,[18,20,34,35] and the changes in the reflectance represented a combination of M/L-cones. The topographic profile showed a high and steep peak of light reflectance increase at the foveal center, which decreased gradually toward the periphery (Fig. 1C).

The green (500 nm) wavelength generally bleaches rods, S-, and M/L-cones,[18,20,34,35] and the topographic changes in reflectance caused by 500 nm light represents the bleaching of all types of photoreceptors. There were high peaks of light reflectance changes at the fovea and the circular region surrounding the macula at an eccentricity of the optic disc (Fig. 1D). The time course of the light reflectance changes was monophasic at the fovea, but biphasic at the temporal retina. The biphasic time course was observed at all retinal locations except for the fovea, and can be explained by the bleaching processes of rod photoreceptors, that is bleaching of 11-cis-retinal to Meta-II intermediates (peak 380 nm) for the initial phase and the bleaching of Meta-III intermediates (peak 465 nm) to all-transretinal and opsin in the late phase.[36,37] These findings indicated that the response topography at the fovea is dominated by bleaching of cones and that in the peripheral region is dominated by bleaching of rods.

Both the S-cones and rods are sensitive to 445 nm,[18,20,34,35] and the topographic changes in the reflectance pattern after bleaching with the green (445 nm) filter represents mainly the bleaching of both rods and S-cones. However, the M/L cones also absorb this wavelength. As with bleaching with 500 nm, the bleaching profile showed that there were peaks of light reflectance changes at the fovea and the circular region surrounding the macula (Fig. 1E). However, the foveal peak was not steep as with 590 or 500 nm but more rounded. This indicated that the reflectance topography at the fovea was not dominated by bleaching of M/L-cones, which should be the maximum at the foveal center. The time course of the light reflectance changes was monophasic at the fovea but biphasic at the temporal retina, as it was with 500 nm. This indicated that the reflectance topography in the peripheral region is dominated by the bleaching of rods.[36,37]

Mapping Rod and S-Cone Responses Based on Bleaching Time Course

The time courses of the reflectance changes during bleaching by 500 nm of different intensities are shown in Figure 2A. With high intensity of 6.54 log scot. tld, the reflectance changes were greater at the fovea (39.9%) than at the temporal retina (20.4%) 8 minutes following the onset of bleaching (Fig. 2A, red line). With low intensity light of 4.73 log scot. tld, the light reflectance changes were lower at the fovea (1.03%) than at the temporal retina (2.28%, Fig. 2A, black line). In addition, during the initial three minutes of bleaching with low intensity light, the foveal response was minimal and remained at 0.1% (Fig. 2B, solid line). This indicated that bleaching of rod photoreceptors could be isolated by measuring the reflectance changes with low light intensity during the initial three minutes. Thus, the topographic distribution of the bleaching of rods could be obtained, and it had a donut-shaped circular

reflectance value at 12.5 sec after the onset (*arrowhead* in **E**) (**F**). The response at the temporal retina remains almost flat between 12.5 to 35.0 seconds in (**F**). (**G, H**) The response topographies for 445 nm at 35.0 seconds shown in (**F**) and (**H**) measured in the perimacular region in (**G**). The color scale indicates the relative reflectance changes (%) at 35.0 minutes to the reflectance at 12.5 minutes. Data from Monkeys 2 and 1 are presented for rod and S-cone, respectively.
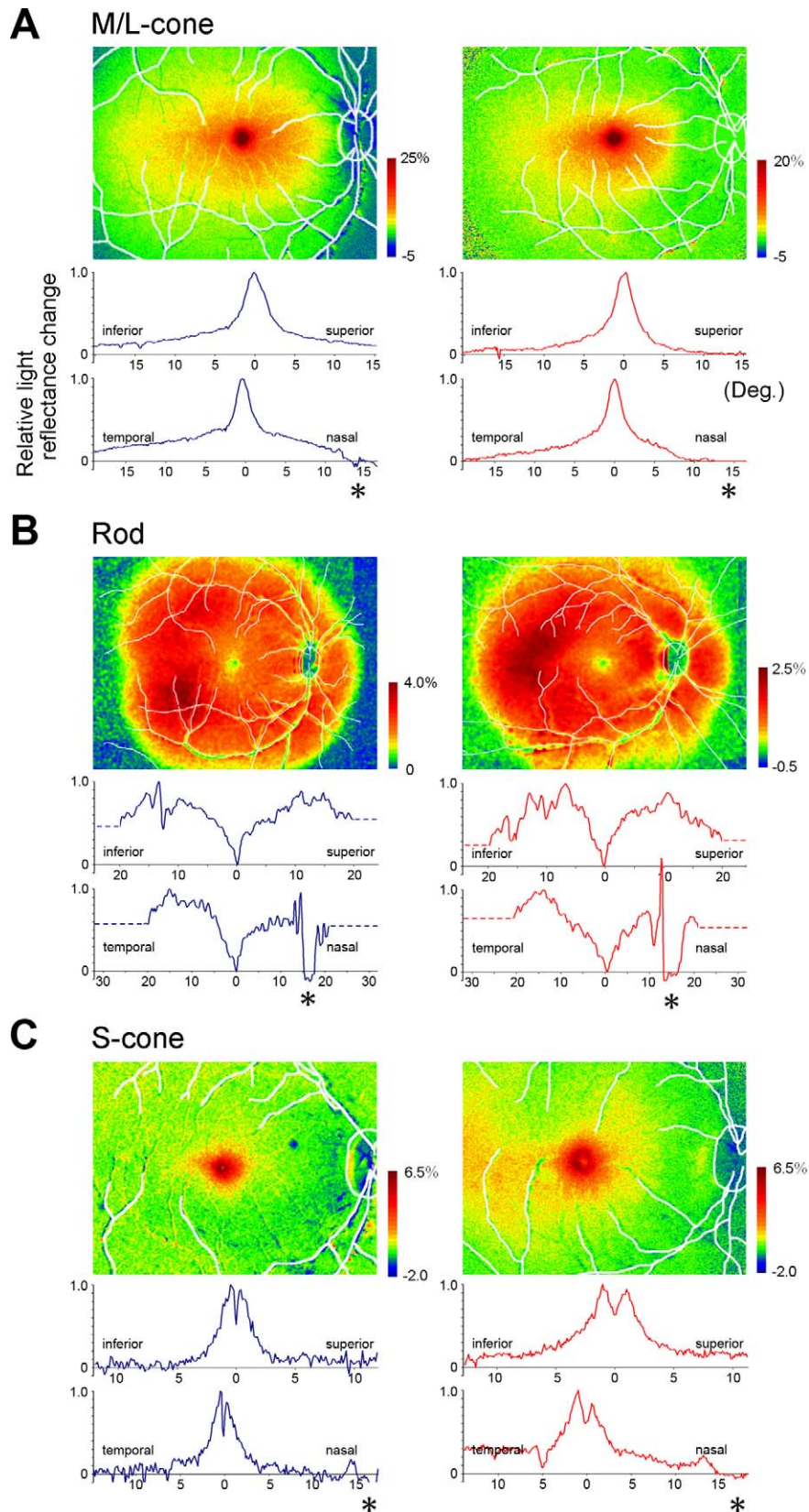
FIGURE 3. Pseudo-color functional topographies for the three types of photoreceptors in two monkeys. (**A–C**) pseudo-colored functional topographic maps for the three types of photoreceptors (*upper*) and relative response values to the peak (1.0) in the vertical and horizontal profile along the foveal center (*lower*). (**A**) Response topographies for the M/L cones obtained by 5.35 log phot. td between 60 to 180 seconds following the illumination. (**B**) Response topographies for the rods obtained by 4.73 log scot. tld between 52.5 to 150 seconds following the illumination. The response profiles outside the region of interest are shown as dotted lines. (**C**) Response topographies for the S-cone, obtained by 4.58 log phot. td between 30 to 60 seconds following the illumination. Locations of the retinal vessels are overlaid by white lines. *Zero* degree in the response profile

pattern with an annular peak at an eccentricity of 9.4 to 14.0 degrees from the fovea (Fig. 2D).

The light reflectance changes with 445 nm of 4.58 log phot. td during the initial 75 seconds are expanded in Figure 2E. The time-course at the temporal retina was flatter 12.5 seconds after the onset of bleaching (Fig. 2E, blue line). The reflectance changes relative to the reflectance value at 12.5 seconds after the onset (arrowhead in Fig. 2E) are re-plotted in Figure 2F. During the initial 22.5 seconds (underlined by gray), the degree of reflectance increased to 13.7% at the fovea (red line), but remained flat at the temporal retina (blue line). The light reflectance at the peripheral region did not increase during this period due to the conversion from Meta-II intermediates (peak 380 nm) to Meta-III intermediates (peak 465 nm) of the rod photopigments.[36,37] These changes indicated that the topography obtained during this period did not reflect the responses of rods but was dominated by S-cones. Thus, the topography of S-cone bleaching in the macula could be obtained, and it had a volcano-shaped activation with the foveal center largely excavated (Fig. 2H). This is considered to reflect the reduced number of S-cones at the fovea.

Functional Topography of M/L Cones, Rods, and S-Cones

By considering the preferred wavelengths and the characteristic time courses of the reflectance changes, we have shown the functional topographies of the M/L-cones, rods and S-cones in two monkeys (Fig. 3) in horizontal and vertical sections. The distribution of M/L-cones response had a steep peak at the foveal center and was elongated horizontally. The distribution of rod responses was minimum at the foveal center and maximum along the circular region at the eccentricity of the optic disc. The distribution of S-cone responses was highest at the fovea and was excavated centrally. There was a circular region with the maximal responses at 0.38 to 1.0 degrees from the foveal center.

DISCUSSION

We determined the functional topographic maps of rods, M/L-cones, and S-cones based on the differences in retinal reflectance changes after a selective bleaching of the photopigments by using a flood illumination camera system. A confocal SLO system also could have been used because it has the better spatial resolution. In addition, the intensity of illumination falling on the retina can be homogeneous and modifications of the optical pathway would not be needed as with the fundus camera. However, the most important part of this study was not the imaging resolution alone, but the ability to obtain functional topographic maps of different types of photoreceptors by using different combinations of wavelengths, stimulus intensities, and stimulus durations (Fig. 2). These combinations allowed us to segregate the responses of the different types of photoreceptors. We conducted preliminary experiments with various band pass interference filters and concluded that the combination of 445, 500, and 590 nm filters was ideal for our purposes. In that sense, the simplicity of a flood illumination camera system was advantageous for us.

In the M/L cones (Fig. 3A), the reflectance pattern was approximately equal to that obtained by anatomical studies in macaque and human retinas.[3,4] The reflectance distribution was elongated horizontally with a peak at the foveal center.

In the rods (Fig. 3B), the reflectance changes were minimal at the foveal center, and increased rapidly toward the periphery. The reflectance distribution had a "rod ring" at the eccentricity of the optic disc, that is 9.4 to 14.0 degrees from the center as has been detected by anatomical studies.[3,4] The vertical gradient toward the superior retina described by Curcio et al.[3,4] could not be observed, but instead, the rod responses were maximum at the temporal region along the rod ring.

In the S-cones (Fig. 3C), the reflectance distribution had a volcano-like excavation at the foveal center. The S-cone-free region at the foveal center has been found in macaques and humans anatomically[2,5,7] and psychophysically.[11,13,38] Our results showed that S-cones are functionally minimal at the foveal center in the macaques. The diameter of the ring-shaped peaks with maximal reflectance changes was 0.83 degrees (vertically) x 0.75 degrees (horizontally) in M1 and 1.99×1.55 degrees in M2 (Fig. 1C). The eccentricities of the S-cone peaks were within the variations of those obtained by anatomical[2,5,7] and psychophysical studies.[11,13,38] The locations of the peaks of the S-cone responses varied among individuals and the ring-shaped peaks looked vertically elongated. We should note that the reflectance topography of S-cones was shown reliably only in the macular region because the S-cone activities in the periphery were relatively small[12] and were cancelled by the rod-induced light reflectance changes (Fig. 2E and 2F).

There are some discrepancies between the results of earlier anatomical studies and our imaging results. This is because the densitometry technique does not depend solely on the density of photoreceptors, but also on the length of photoreceptor outer segments, that is density of photopigments in each photoreceptor. The goal of our study, however, was not to map the density of the photoreceptors, which has been done already through the series of studies by Curcio et al.,[3–5] but to draw the activity-dependent topography of the photoreceptors, which may confirm and augment the response topography obtained by, for example, mutifocal ERGs.

In our technique of fundus reflectometry, the optical pathway was adjusted to illuminate the posterior retina homogeneously so that the results reflected the relative reflectance distribution more accurately. However, there are some possible artifacts by which the reflectance changes may be either over- or underestimated in particular regions. First, the presence of scattered light from the inner limiting membrane and nerve fiber layer around the macula may cause an underestimation of the bleach-induced light reflectance changes.[31] A quantitative evaluation of this scattering effect was very difficult to obtain because the topographies we had presented did not seem to be affected by such artifacts in the peri-macular regions (Fig. 3A).

Second, the effect of intrinsic optical signals, which reflect the hemoglobin-induced light reflectance changes following neural activation, must be considered.[39,40] The intrinsic signals also would be observed in the retina as stimulus-induced light reflectance decreases.[41–43] The intrinsic signals are prominent at a wavelength with the maximum hemoglobin absorption (540–580 nm), and in our response topographies, regions corresponding to the optic disc and large retinal vessels, which are rich in red blood cells, might have had relatively smaller reflectance increases due to the intrinsic signals (Figs. 1 and 3). The maximal light reflectance decrease due to intrinsic signals

indicates the location of fovea. The location of the optic disk is indicated by an asterisk. Data from Monkeys 1 and 3 for M/L cone, Monkeys 2 and 3 for rods, and Monkeys 1 and 2 for S-cones are presented.

in our recording protocol, however was estimated to be 1.0% to 2.0% at the optic disc, where intrinsic signals could be solely and maximally observed.[42] Thus, the intrinsic signals probably had little effect on the overall bleaching topographies.

Third, the Stiles-Crawford effect,[44] the directional sensitivity of the cone photoreceptors, may change the reflectance intensities depending on the position of the illumination center over the retina. In the horizontal response profiles of S-cones (Fig. 3C), the circular peak response was slightly higher in the temporal fovea than in the nasal fovea. This was considered to reflect the Stiles-Crawford effect because the illumination was centered 2.56 degrees temporal to the foveal center, and the rays of light passed cone photoreceptors less oblique at the temporal fovea than at the nasal fovea.

The bleach-induced reflectance changes are affected by such artifacts and may not reflect the distribution of photoreceptor activities accurately.

A clinical application of this technique may not be easy because subjects must keep staring at the fixation target with very bright background illumination for relatively long times. However, there are recent reports using SLO[31,45,46] or a snapshot imaging system[33] to measure cone- or rod-induced response topography. Unfortunately, the response distribution of rods or S-cone responses cannot be extracted accurately as in this study. Our results will provide us with valuable photoreceptor activities in macaque retinas, which can complement those obtained either anatomically[2-5,7] or psychophysically.[10-15,38]

References

1. Osterberg G. Topography of the layer of rods and cones in the human retina. *Acta Ophthalmol*. 1935;13:6-97.

2. de Monasterio FM, McCrane EP, Newlander JK, Schein SJ. Density profile of blue-sensitive cones along the horizontal meridian of macaque retina. *Invest Ophthalmol Vis Sci*. 1985; 26:289-302.

3. Packer O, Hendrickson AE, Curcio CA. Photoreceptor topography of the retina in the adult pigtail macaque (Macaca nemestrina). *J Comp Neurol*. 1989;288:165-183.

4. Curcio CA, Sloan KR, Kalina RE, Hendrickson AE. Human photoreceptor topography. *J Comp Neurol*. 1990;292:497-523.

5. Curcio CA, Allen KA, Sloan KR, et al. Distribution and morphology of human cone photoreceptors stained with anti-blue opsin. *J Comp Neurol*. 1991;312:610-624.

6. Mollon JD, Bowmaker JK. The spatial arrangement of cones in the primate fovea. *Nature*. 1992;360:677-679.

7. Bumsted K, Hendrickson A. Distribution and development of short-wavelength cones differ between Macaca monkey and human fovea. *J Comp Neurol*. 1999;403:502-516.

8. Andrade da Costa BL, Hokoc JN. Photoreceptor topography of the retina in the New World monkey Cebus apella. *Vision Res*. 2000;40:2395-2409.

9. Cornish EE, Hendrickson AE, Provis JM. Distribution of short-wavelength-sensitive cones in human fetal and postnatal retina: early development of spatial order and density profiles. *Vision Res*. 2004;44:2019-2026.

10. Wald G. The receptors of human color vision. *Science*. 1964; 145:1007-1016.

11. Wald G. Blue-blindness in the normal fovea. *J Opt Soc Am*. 1967;57:1289-1301.

12. Wooten BR, Wald G. Color-vision mechanisms in the peripheral retinas of normal and dichromatic observers. *J Gen Physiol*. 1973;61:125-145.

13. Castaño JA, Sperling HG. Sensitivity of the blue-sensitive cones across the central retina. *Vision Res*. 1982;22:661-673.

14. Birch DG, Herman WK, deFaller JM, Disbrow DT, Birch EE. The relationship between rod perimetric thresholds and full-field rod ERGs in retinitis pigmentosa. *Invest Ophthalmol Vis Sci*. 1987;28:954-965.

15. Pulos E. Changes in rod sensitivity through adulthood. *Invest Ophthalmol Vis Sci*. 1989;30:1738-1742.

16. Rushton WA. The rhodopsin density in the human rods. *J Physiol*. 1956;134:30-46.

17. Hood C, Rushton WA. The Florida retinal densitometer. *J Physiol*. 1971;217:213-229.

18. Brown PK, Wald G. Visual pigments in human and monkey retinas. *Nature*. 1963;200:37-43.

19. Rushton WA. Cone pigment kinetics in the protanope. *J Physiol*. 1963;168:374-388.

20. Brown PK, Wald G. Visual pigments in single rods and cones of the human retina. direct measurements reveal mechanisms of human night and color vision. *Science*. 1964;144:45-52.

21. Alpern M, Maaseidvaag F, Oba N. The kinetics of cone visual pigments in man. *Vision Res*. 19771;11:539-549.

22. Alpern M. Rhodopsin kinetics in the human eye. *J Physiol*. 1971;217:447-471.

23. Mizuno K, Majima A, Ozawa K, Ito H. Red-free light fundus photography. Photographic optogram. *Invest Ophthalmol*. 1968;7:241-249.

24. Highman VN, Weale RA. Rhodopsin density and visual threshold in retinitis pigmentosa. *Am J Ophthalmol*. 1973; 75:822-832.

25. Sheorey UB. Clinical assessment of rhodopsin in the eye. Using a standard fundus camera and a photographic technique. *Br J Ophthalmol*. 1976;60:135-141.

26. Kilbride PE, Read JS, Fishman GA, Fishman M. Determination of human cone pigment density difference spectra in spatially resolved regions of the fovea. *Vision Res*. 1983;23:1341-1350.

27. Kilbride PE, Keehan KM. Visual pigments in the human macula assessed by imaging fundus reflectometry. *Appl Opt*. 1990;29: 1427-1435.

28. Faulkner DJ, Kemp CM. Human rhodopsin measurement using a T.V.-based imaging fundus reflectometer. *Vision Res*. 1984; 24:221-231.

29. Kemp CM, Faulkner DJ, Jacobson SG. The distribution and kinetics of visual pigments in the cat retina. *Invest Ophthalmol Vis Sci*. 1988;29:1056-1065.

30. van Norren D, van de Kraats J. Imaging retinal densitometry with a confocal Scanning Laser Ophthalmoscope. *Vision Res*. 1989;29:1825-1830.

31. Elsner AE, Burns SA, Hughes GW, Webb RH. Reflectometry with a scanning laser ophthalmoscope. *Appl Opt*. 1992;31: 3697-3710.

32. Berendschot TT, DeLint PJ, van Norren D. Fundus reflectance-historical and present ideas. *Prog Retin Eye Res*. 2003;22:171-200.

33. Kazato Y, Shibata N, Hanazono G, Suzuki W, Tanifuji M, Tsunoda K. Novel snapshot imaging of photoreceptor bleaching in macaque and human retinas. *Jpn J Ophthalmol*. 2010;54:349-356.

34. Bowmaker JK, Dartnall HJ. Visual pigments of rods and cones in a human retina. *J Physiol*. 1980;298:501-511.

35. Bowmaker JK, Dartnall HJ, Mollon JD. Microspectrophotometric demonstration of four classes of photoreceptor in an old world primate, Macaca fascicularis. *J Physiol*. 1980;298:131-143.

36. Imai H, Kuwayama S, Onishi A, Morizumi T, Chisaka O, Shichida Y. Molecular properties of rod and cone visual pigments from purified chicken cone pigments to mouse rhodopsin in situ. *Photochem Photobiol Sci*. 2005;4:667-674.

37. Shichida Y, Imai H, Imamoto Y, Fukada Y, Yoshizawa T. Is chicken green-sensitive cone visual pigment a rhodopsin-like pigment - a comparative-study of the molecular-properties between chicken green and rhodopsin. *Biochemistry*. 1994; 33:9040–9044.

38. Williams DR, MacLeod DI, Hayhoe MM. Punctate sensitivity of the blue-sensitive mechanism. *Vision Res*. 1981;21:1357–1375.

39. Grinvald A, Lieke E, Frostig RD, Gilbert CD, Wiesel TN. Functional architecture of cortex revealed by optical imaging of intrinsic signals. *Nature*. 1986;324:361–364.

40. Bonhoeffer T, Grinvald A. Optical imaging based on intrinsic singals: the methodology. In: Toga AW, Mazziotta JC, eds. *Brain Mapping*. San Diego: Academic Press; 1996:55–97.

41. Tsunoda K, Oguchi Y, Hanazono G, Tanifuji M. Mapping cone- and rod-induced retinal responsiveness in macaque retina by optical imaging. *Invest Ophthalmol Vis Sci*. 2004;45:3820–3826.

42. Hanazono G, Tsunoda K, Kazato Y, Tsubota K, Tanifuji M. Evaluating neural activity of retinal ganglion cells by flash-evoked intrinsic signal imaging in macaque retina. *Invest Ophthalmol Vis Sci*. 2008;49:4655–4663.

43. Tsunoda K, Hanazono G, Inomata K, Kazato Y, Suzuki W, Tanifuji M. Origins of retinal intrinsic signals: a series of experiments on retinas of macaque monkeys. *Jpn J Ophthalmol*. 2009;53:297–314.

44. Stiles WS, Crawford BH. The luminous efficiency of rays entering the eye pupil at different points. *Proc Roy Soc London Series B-Containing Papers of a Biological Character*. 1933;112:428–450.

45. Elsner AE, Burns SA, Beausencourt E, Weiter JJ. Foveal cone photopigment distribution: small alterations associated with macular pigment distribution. *Invest Ophthalmol Vis Sci*. 1998;39:2394–2404.

46. Sekiryu T, Iida T, Maruko I, Horiguchi M. Clinical application of autofluorescence densitometry with a scanning laser ophthalmoscope. *Invest Ophthalmol Vis Sci*. 2009;50:2994–3002.